STRUCTURAL CHEMISTRY

ISSN 2053-2296

Syn- and *anti*-rotamers of the *ortho*-stereoisomer [Pt{(*o*-BrC_6F_4)N(CH_2)$_2$$NEt_2$}Cl(py)]

Ruchika Ojha,[a,b] Alan M. Bond,[a]* Peter C. Junk[c]* and Glen B. Deacon[a]*

[a]School of Chemistry, Monash University, VIC 3800, Australia, [b]School of Science, STEM College, RMIT University, Melbourne, VIC 3000, Australia, and [c]College of Science & Engineering, James Cook University, Townsville, Qld 4811, Australia. *Correspondence e-mail: alan.bond@monash.edu, peter.junk@jcu.edu.au, glen.deacon@monash.edu

Received 23 July 2025
Accepted 30 July 2025

Edited by M. Yousufuddin, University of North Texas at Dallas, USA

Keywords: crystal structure; platinum anticancer agent; *syn* and *anti* rotamers; agostic interactions; synchrotron.

CCDC references: 2481234; 2477306

Supporting information: this article has supporting information at journals.iucr.org/c

The crystal structure of the *ortho*-isomer *trans*-[*N*-(2-bromo-3,4,5,6-tetrafluorophenyl)-*N*′,*N*′-diethylethane-1,2-diaminato(1−)]chloridopyridineplatinum(II), [$PtBr_{0.1}(C_{12}H_{14}BrF_4N_2)Cl_{0.9}(C_5H_5N)$][$PtBr_{0.4}(C_{12}H_{14}BrF_4N_2)Cl_{0.6}(C_5H_5N)$] or [Pt{(*o*-$BrC_6F_4$)N($CH_2$)$_2$$NEt_2$}Cl(py)], **1*o***, revealed *syn* and *anti* rotamers in a 1:1 ratio in the solid state. **1*o*** crystallizes in the centrosymmetric space group $P\overline{1}$. The Pt-coordinated Cl ligand exhibits partial occupancy with Br, predominantly in the *syn*-rotamer. Notably, agostic interactions are observed between the Pt centre and a H atom of one of the ethyl groups. The *ortho*-isomer **1*o*** was successfully isolated as a side product from the reaction of [Pt{H_2N(CH_2)$_2$$NEt_2$}$Cl_2$], Tl_2CO_3 and C_6F_5Br. While the *para*-isomer [Pt{(*p*-BrC_6F_4)N(CH_2)$_2$$NEt_2$}Cl(py)], **1*p***, is the main product, the higher solubility of **1*o*** facilitates its isolation.

1. Introduction

Polyfluoroaryl-substituted organoamidoplatinum(II) complexes [Pt{*R*N(CH_2)$_2$N*R*′$_2$}*X*(py)] [*R* = *p*-*Y*C_6F_4 (*Y* = F, Cl, Br or I), CH_3, *etc.*; *R*′ = Me or Et; *X* = Cl, Br or I; py = pyridine] have been shown to have good *in vitro* and modest *in vivo* activity (Talarico *et al.*, 1999; Ojha *et al.*, 2021) against a number of tumour cells. They are conveniently prepared by reaction of [Pt*X*$_2$($NH_2CH_2CH_2$N*R*′$_2$)] with thallium(I) carbonate (or K_2CO_3 in some cases) and a polyfluoroarene, *R*F, in boiling pyridine (Fig. 1) (Battle *et al.*, 2010; Ojha *et al.*, 2015). The CO_2 generated from Tl_2CO_3 during the reaction was trapped as $BaCO_3$ by a $Ba(OH)_2$ solution, and the yield of CO_2 was measured gravimetrically.

One step in the complex CO_2 elimination reaction paths is nucleophilic substitution of F on the polyfluorobenzene, *R*F, by the $–NH_2$ group, plausibly partially deprotonated by the carbonate group. The substitution pattern of the major products (Battle *et al.*, 2010; Buxton *et al.*, 1988; Deacon *et al.*, 1991) corresponds to that (*para* to substituent *Y*), as observed in the nucleophilic substitution of polyfluoroarenes (Chambers *et al.*, 1974, 1977; Chambers, 2004). Although the ^{19}F NMR spectra of crude reaction products sometimes suggested that the reactions were not entirely regiospecific, simple recrystallization usually gave isomerically pure products (Battle *et al.*, 2010; Buxton *et al.*, 1988; Deacon *et al.*, 1991). However, the reaction of [$PtCl_2$(en)] (en is ethylenediamine), Tl_2CO_3 and 2-bromo-1,3,4,5-tetrafluorobenzene in pyridine gave isomers with the N atom *para* to both H and Br. Only the former was isolated, the latter being identified spectroscopically in the reaction mixture (Battle *et al.*, 2010).

We have recently reported anticancer activity (Ojha *et al.*, 2021), chemical oxidation (Ojha *et al.*, 2023) and the synthesis

of [Pt{(*p*-BrC$_6$F$_4$)N(CH$_2$)$_2$NEt$_2$}Cl(py)], **1*p*** (with *X* = Cl, *R*′ = Et and *R* = *p*-BrC$_6$F$_4$), in 64% yield by reaction between [PtCl$_2${H$_2$N(CH$_2$)$_2$NEt$_2$}], Tl$_2$CO$_3$ and C$_6$F$_5$Br in pyridine (Fig. 2) (Ojha *et al.*, 2015). During this study, it was noticed that the hexane washings of the crude product (to remove adherent pyridine) had a yellow colour. We have now investigated the source of the colour and have isolated and crystallized the *ortho*-isomer, [Pt{(*o*-BrC$_6$F$_4$)N(CH$_2$)$_2$NEt$_2$}Cl(py)], **1*o***. This has been identified by X-ray crystallography, employing synchrotron radiation, and found to crystallize as a 1:1 mixture of the *syn* (**1*ox***) and *anti* (**1*oy*)** rotamers (with respect to the *o*-Br and Pt—Cl positions) in the asymmetric unit.

2. Experimental

2.1. General

NMR spectra were recorded in deuterated acetone with a Bruker DPX 400 spectrometer supported by *Top Spin* NMR software on a Windows NT workstation. CFCl$_3$ and tetramethylsilane (TMS) were used for the internal calibration of the ^{19}F NMR and ^{1}H NMR spectra, respectively. IR spectra were recorded on a Perkin–Elmer 1600 FT–IR spectrophotometer as Nujol and hexachlorobutadiene (HCB) mulls between NaCl plates or recorded with an Agilent Cary 630 attenuated total reflectance (ATR) spectrometer in the range 4000–600 cm^{-1}.

2.2. X-ray crystallography

Crystal data, data collection and structure refinement details are summarized in Table 1. X-ray diffraction data obtained from single crystals of **1*ox*/1*oy*** were collected at a wavelength of λ = 0.712 Å using the MX1 beamline at the Australian Synchrotron, Victoria, Australia, with a *Blue Ice* (McPhillips *et al.*, 2002) GUI, using the same method as mentioned in the *Experimental* section of Ojha *et al.* (2015). Data were processed with the *XDS* (Kabsch, 1993) software package. Single crystals were loaded onto a fine glass fiber or cryoloop using hydrocarbon oil, with the collection kept at 123 K using an Oxford Cryosystems open-flow N$_2$ Cryostream. The program *OLEX2* (Dolomanov *et al.*, 2009) was used as the graphical interface. H atoms attached to C atoms were placed in calculated positions and allowed to ride on the atom to which they were attached.

Table 1
Crystallographic data for the molecular structures of **1*ox*/1*oy*** and comparison with **1*p***.

	ortho-**1*ox*/1*oy***	**1*p*** (Ojha *et al.*, 2015)
Empirical formula	$C_{34}H_{38}Br_{2.5}Cl_{1.5}F_8N_6Pt_2$	$C_{17}H_{19}BrClF_4N_3Pt$
Formula weight	1321.39	651.78
Crystal system	Triclinic	Monoclinic
Space group	$P\overline{1}$	$P2_1/c$
a (Å)	9.4810 (19)	10.960 (2)
b (Å)	14.656 (3)	11.961 (2)
c (Å)	15.094 (3)	15.224 (3)
α (°)	75.02 (3)	90
β (°)	74.62 (3)	98.46 (3)
γ (°)	86.28 (3)	90
V (Å^3)	1953.5 (8)	1974.0 (7)
Z	2	4
ρ (calcd) (Mg m^{-3})	2.246	2.193
μ (mm^{-1})	9.790	9.311
F(000)	1246.0	1232
Reflections collected/unique	24773/8572	22718/3354
R_{int}	0.0553	0.0267
$2\theta_{max}$ (°)	55.8	50.0
Goodness-of-fit on F^2	1.052	1.126
*R*1 indices [$I > 2\sigma(I)$]	0.0626	0.0217
*wR*2 indices	0.1743	0.0518

Computer programs: *Blue Ice* (McPhillips *et al.*, 2002), *XDS* (Kabsch, 1993), *SHELXT2014* (Sheldrick, 2015*a*) and *SHELXL2018* (Sheldrick, 2015*b*).

2.3. Isolation of *ortho*-isomers [Pt{(*o*-BrC$_6$F$_4$)NCH$_2$CH$_2$NEt$_2$}Cl(py)], 1*ox*/1*oy*

After completion of the typical synthesis of **1*p*** by a CO$_2$ elimination reaction (Ojha *et al.*, 2015), pyridine was removed under vacuum until dryness. Hexane was added to remove traces of residual pyridine and decanted. The major product **1*p*** was extracted with acetone from the remaining solid, as reported earlier. The decanted hexane was yellow–orange, rather than colourless, indicating that it had not just removed the remaining pyridine, but possibly an isomer.

To isolate and crystallize the isomers, some acetone was added to the decanted solution. Crystals of **1*ox*/1*oy*** suitable for structure determination were obtained by slow evaporation of the solvent. **1*ox*** and **1*oy*** are present in a 1:1 ratio. Apart from the X-ray data, the integrations for ^{1}H resonances measured in (CD$_3$)$_2$CO show **1*ox*/1*oy*** in a 1:1 ratio.

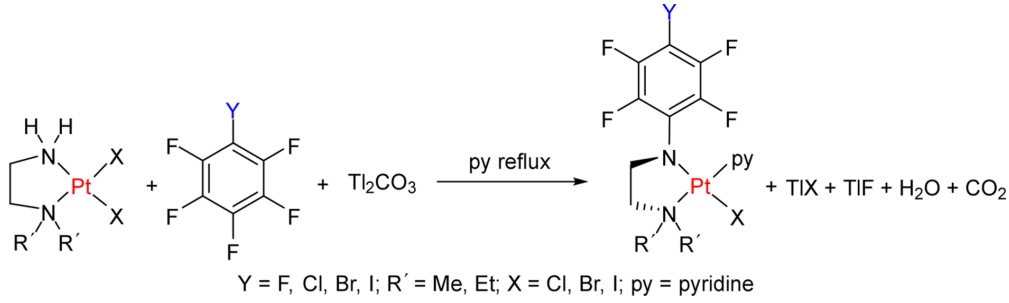

Figure 1
General synthesis of [Pt{*R*N(CH$_2$)$_2$N*R*′$_2$}*X*(py)].

Table 2
Observed and calculated chemical shifts (ppm) for **1*o*** and their comparison with calculated *m*-BrC_6F_4 organoamidoplatinum(II) compounds.

F	Observed	Calculated for *o*-BrC_6F_4	F	Calculated for *m*-BrC_6F_4
F3	−140.6	−140.6	F2	−122.5
F6	−151.2	−151.1	F6	−145.1
F5	−160.9	−163.2	F4	−145.2
F4	−171.1	−174.8	F5	−169.2

Metallic yellow–orange blocks (yield: 0.130 g, 20%). ^{19}F NMR [$(CD_3)_2CO$]: δ −140.6 (*d*, 2F, F3), −151.2 (*d*, 2F, F6), −160.9 (*t*, 2F, F5), −171.1 (*m*, 2F, F4). ^{1}H NMR [$(CD_3)_2CO$]: δ 1.53 (*t*, $^3J_{H,H}$ = 7.15 Hz, 12H, $NCH_2C\mathbf{H_3}$), 2.48 (*t*, with ^{195}Pt–H satellites, $^3J_{H,H}$ = 6, $^3J_{H,Pt}$ = 30 Hz, 4H, $C\mathbf{H_2}NEt_2$), 2.80 (*m*, 4H, NC**HA**HBCH_3), 3.34 [*m*, 8H, made up of 4H $C\mathbf{H_2}N$(*p*-BrC_6F_4) and 4H NC**HB**HACH_3], 7.09 [*t*, $^3J_{H,H}$ = 7 Hz, 2H, **H3,5**(py)], 7.15 [*t*, 2H, $^3J_{H,H}$ = 7 Hz, **H3,5**(py)], 7.65 [*tt*, $^3J_{H,H}$ = 7, $^4J_{H,H}$ = 1 Hz, 1H, **H4** (py)], 7.70 [*tt*, $^3J_{H,H}$ = 7, $^4J_{H,H}$ = 1 Hz, 1H, **H4** (py)], 8.50 [*d* with ^{195}Pt–H satellites, $^3J_{H,H}$ = 5, $^3J_{H,Pt}$ = 36 Hz, 2H, **H2,6**(py)], 8.54 [*d* with ^{195}Pt–H satellites, $^3J_{H,H}$ = 5, $^3J_{H,Pt}$ = 36 Hz, 2H, **H2,6**(py)]. IR (cm^{-1}): 2960 (*w*), 2922 (*w*), 2853 (*w*), 1654 (*w*), 1618 (*w*), 1607 (*b*), 1458 (*s*), 1450 (*s*), 1375 (*m*), 1345 (*w*), 1258 (*s*), 1208 (*m*), 1133 (*s*), 1073 (*s*), 1014 (*s*), 962 (*s*), 898 (*m*), 875 (*m*), 794 (*s*), 765 (*s*), 691 (*s*).

3. Results and discussion

The *ortho*-isomer **1*o*** was preferentially isolated due to its markedly greater solubility in hexane compared to the *para*-isomer **1*p***. The synthesis predominantly afforded **1*p*** (Ojha *et al.*, 2015) by a CO_2 elimination reaction (Fig. 2). A subsequent hexane washing, intended to remove residual pyridine, unexpectedly exhibited a yellow–orange coloration. This observation suggested the presence of an additional platinum-containing species, which could be a different isomer, rather than merely solvent. Therefore, it was investigated further, and slow evaporation of the hexane washing enabled the isolation of the *ortho*-isomer [Pt{(*o*-BrC_6F_4)$NCH_2CH_2NEt_2$}Cl(py)], **1*o***, which was considerably more soluble in the low-polarity solvent hexane (with a trace of pyridine) than **1*p***. The *ortho*-isomer **1*o*** crystallized as a 1:1 mixture of the *anti* (**1*ox***) and *syn* (**1*oy***) rotamers in the asymmetric unit. This procedure facilitates isolation of the pure *para*-isomer (**1*p***) as the major product from the reaction mixture.

3.1. Characterization of 1*o*

The initial identification of **1*o*** was *via* ^{1}H and ^{19}F NMR spectroscopy in $(CD_3)_2CO$. The coordination of pyridine and the amide ligand to platinum was evident from the observation of $^3J(^{195}Pt,H)$ satellites (^{195}Pt isotope, nuclear spin I = 1/2, natural abundance = 33.8%) on the signals of the H2,6(pyridine) and CH_2(N-ethyl) protons, with the coupling constants ^3J(Pt,H2,6-py) and ^3J(Pt,CH_2-N) having values (36 and 30 Hz, respectively) similar to those (35 and 28 Hz) observed for **1*p*** (Ojha *et al.*, 2015). Other ^{1}H chemical shifts and integrations, which are similar to those of **1*p***, are consistent with the composition of **1*o***.

Evidence for the proposed polyfluorophenyl substitution pattern comes from ^{19}F NMR spectroscopy. Four equal-intensity ^{19}F resonances indicate either a *m*-BrC_6F_4 or an *o*-BrC_6F_4 group compared with two for **1*p*** (Fig. S1 for the F-atom numbering system). Chemical shift calculations {based on substituent chemical shifts for Br (Bruce, 1968; Ando & Matsuura, 1995), for *o*- and *m*-[N(–CH_2)Pt] groups derived from **1*p*** (Ojha *et al.*, 2015), and for *p*-[N(CH_2–)Pt] derived from several [Pt{$C_6F_5NCH_2CH_2NEt_2$}*X*(py)] complexes (Deacon *et al.*, 1991)] clearly support the presence of an *o*-BrC_6F_4 substituent in **1*o***, and compares well with the observed chemical shift (Table 2). The ^{19}F NMR spectrum is provided in the supporting information (Fig. S2) and shows the same chemical shifts for **1*ox*** and **1*oy***. In the ^{1}H NMR spectrum, the pyridine resonances in **1*ox*** and **1*oy*** appear 0.1 ppm apart, as shown in Fig. S3, and show **1*ox*** and **1*oy*** in a 1:1 ratio.

The unequivocal identification of **1*o*** was provided by X-ray crystallography. The crystallographic data differ considerably from those of **1*p*** (Table 1). **1*o*** crystallizes in the triclinic space

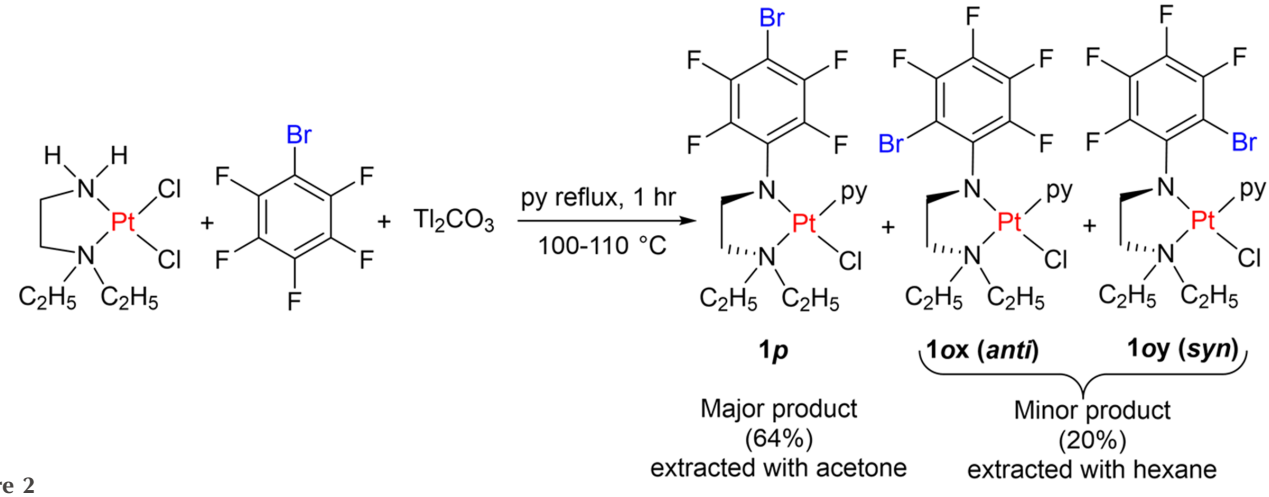

Figure 2
Carbon dioxide elimination reaction for the synthesis of **1*p*** and **1*ox*/1*oy***.

Table 3
Selected bond lengths (Å) and bond angles (°) for **1*ox*/1*oy*** and comparison with **1*p***.

Bond	**1*ox***	**1*oy***	**1*p***	Angle	**1*ox***	**1*oy***	**1*p***
Pt—Cl	2.35 (3)	2.323 (7)	2.344 (10)	Cl—Pt—N(amide)	177.5 (9)	175.8 (4)	176.17 (9)
Pt—Br	2.534 (16)	2.62 (3)	–	N(amide)—Pt—N(Et_2)	84.2 (4)	83.5 (4)	82.65 (12)
Pt—N(amide)	1.993 (11)	2.006 (11)	2.006 (3)	N(amide)—Pt—N(py)	91.6 (4)	93.2 (4)	93.27 (12)
Pt—N(Et_2)	2.087 (10)	2.076 (9)	2.074 (3)	Cl—Pt—N(Et_2)	93.3 (8)	92.3 (4)	93.98 (9)
Pt—N(py)	2.034 (9)	2.026 (9)	2.013 (3)	Cl—Pt—N(py)	90.9 (8)	90.9 (4)	90.25 (8)
N(amide)—C(C_6F_4)	1.383 (19)	1.362 (19)	1.354 (4)	N(Et_2)—Pt—N(py)	174.8 (4)	173.8 (4)	173.53 (12)

group $P\bar{1}$ with the rotamers **1*ox*** and **1*oy*** (Fig. 2) in the asymmetric unit (Table 1). In **1*ox***, Br and Cl are *anti* with a Br—Pt—Cl angle of 156.86 (6)°, whereas in **1*oy***, they are in a *syn* disposition with a Br—Pt—Cl angle of 113.61 (8)°.

In the proposed mechanism, initially, both chloride ligands on Pt are replaced by pyridine. Due to the hydrogen bonding between –NH_2 and CO_3^{2-}, a lone-pair character is generated on the N atom and initiates nucleophilic substitution in the polyfluoroaryl ring (Deacon *et al.*, 1998), as shown in Scheme S1 in the supporting information.

The Meisenheimer intermediates involved in the formation of **1*p*** and **1*o*** are depicted in Fig. 3. In the case of **1*p***, the negative charge generated during the nucleophilic substitution of the polyfluoroaryl ring is stabilized by two *ortho*- and two *meta*-fluorines, relative to the site of substitution (see Scheme S2 in the supporting information). Similarly, the formation of the *ortho*-Br isomers is also feasible because the negative charge in the Meisenheimer intermediate (Fig. 3) is located *para* and *ortho* to the site of substitution. This causes the positions *ortho* and *para* to Br to be electron deficient and thus susceptible to nucleophilic attack (Scheme S2). The negative charge in the Meisenheimer intermediate is stabilized by two *o*-F and two *m*-F atoms in **1*p***, and by two *o*-F and one *m*-F atom in **1*o***.

The displacement of the pyridine ligand *trans* to the amide group by the chloride ion gives the target compound (see Scheme S1 in the supporting information). This regiospecificity is obtained as the *trans* effect of the –N(*p*-BrC_6F_4) N atom is greater than that of the –NEt_2 N atom, in line with the *trans*-influence values from platinum–H coupling constants (Buxton *et al.*, 1988).

In **1*ox***, the Cl ligand coordinated to the Pt atom has a shared occupancy with Br, *cf.* 0.59 (1):0.41 (1), yielding 0.59 Cl and 0.41 Br, while for **1*oy***, the Cl remains the major occupant, with 0.91 (1) Cl and a slight sharing 0.09 (1) with Br. The Br atom is derived from C_6F_5Br. It has previously been shown that some elimination of Br occurs during the oxidation of **1*p*** by hydrogen peroxide (Ojha *et al.*, 2021), and replacement of chloride coordinated to Pt by bromide is consistent with the stability constants for soft metals (Ault *et al.*, 1977).

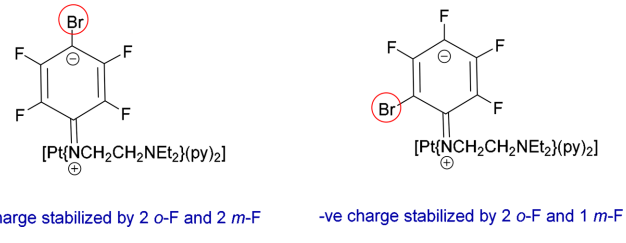

Figure 3
The Meisenheimer intermediates formed during the formation of **1*p*** (left) and **1*o*** (right).

The molecular structure of **1*o*** shows that the Pt atom is coordinated in a square-planar array by a chelating {(*o*-Br-C_6F_4)$NCH_2CH_2NEt_2$}$^-$, pyridine and chloride ligands, with the chloride ligand being *trans* to the amide N atom and pyridine being *trans* to the amine group (Fig. 4). Thus, it is a *trans*-isomer in terms of the positions of the like-charged donor atoms. Selected bond lengths and angles for **1*ox*/1*oy*** are given in Table 3 and compared with those of **1*p***. In general, the values for **1*ox*/1*oy*** and **1*p*** agree within or near the 3 e.s.d. level. However, the Pt—Cl bond of **1*ox*** is longer than that of **1*oy*** or **1*p***, owing to the shared Cl/Br occupancy. This is not a steric effect as the bond does not appear crowded. Supramolecular effects need to be considered. The Pt—N bond lengths follow the sequence Pt—N(amide) < Pt—N(py) < Pt—N(Et_2) (Table 3), as was also observed for **1*p***. Most bond angles around the Pt centre are 90°, with the smallest being the bite angles of 84.1° for **1*ox*** and 83.5° for **1*oy***. The –NCH_2—CH_2N– sawhorse backbone is crooked, as seen in **1*p*** and other compounds of this class (Deacon *et al.*, 1991; Ojha *et al.*, 2016).

Intramolecular hydrogen bonding in **1*ox*** is observed as (NEt_2)H···Br, with an H···Br distance of 2.91 (2) Å, while

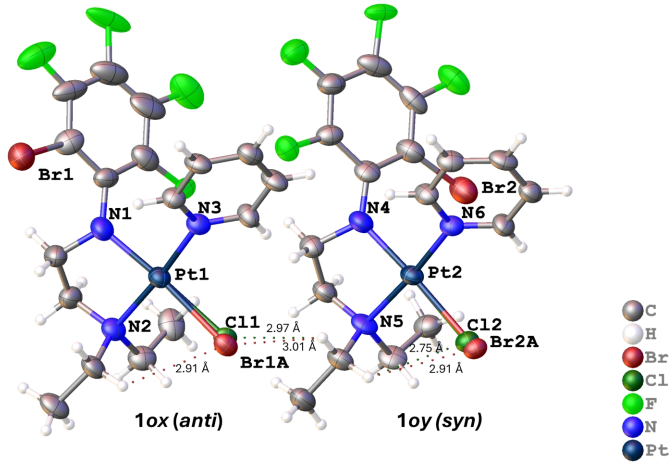

Figure 4
The molecular crystal structures of rotamers **1*ox*** (*anti*) and **1*oy*** (*syn*) cocrystallized in a single unit cell, showing 50% probability displacement ellipsoids.

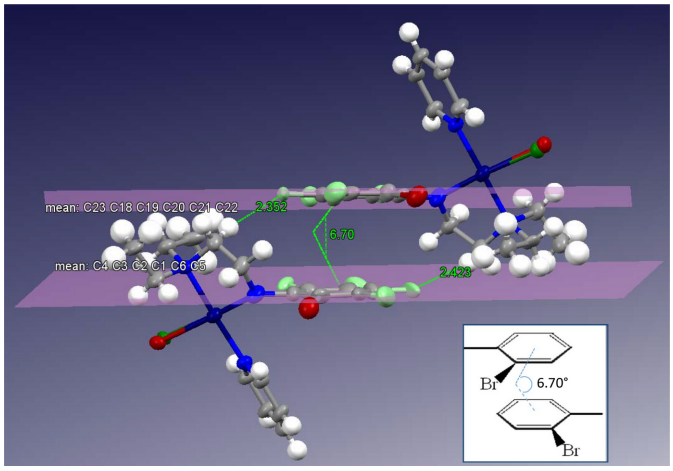

Figure 5
The π–π interaction between the two polyfluoroaryl rings of two molecules with an angle of 6.703 (3)°, where the mirror image is rotated by 180° and the symmetry code is $(-x+1, -y, -z+1)$. The inset shows the *ortho*-Br atoms.

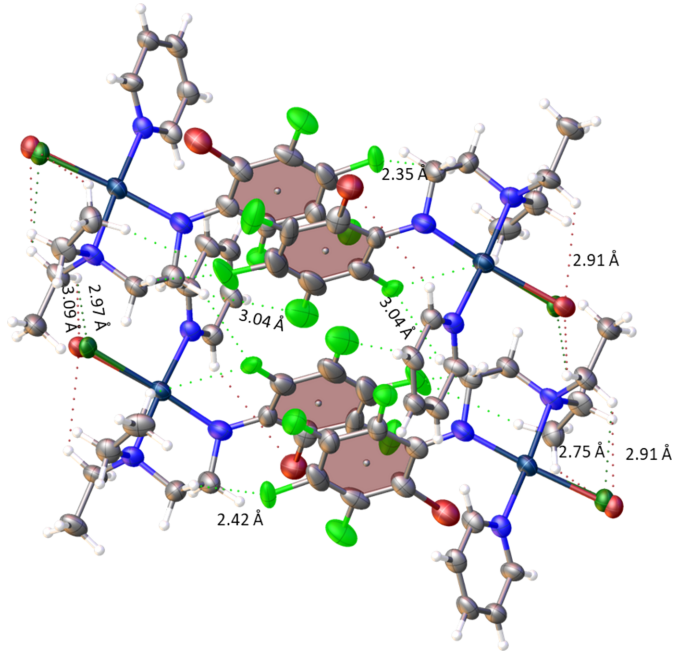

Figure 6
The crystal packing in **1*ox***/**1*oy***, showing the π–π interactions between the two polyfluoroaryl rings of **1*ox*** and **1*oy***, and inter- and intramolecular hydrogen bonding.

1*oy* displayed an $(NEt_2)H\cdots Br$ interaction of 2.91 (4) Å and an $(NEt_2)H\cdots Cl$ interaction of 2.754 (9) Å (Fig. 4). Intermolecular hydrogen bonding between the **1*ox*** Cl/Br atoms and the $H(NEt_2)$ atom of **1*oy***, with an $(NEt_2)H\cdots Br$ distance of 3.093 (19) Å and an $(NEt_2)H\cdots Cl$ distance of 2.97 (3) Å, was also observed. A π–π interaction between the two polyfluoroaryl rings is present (but not between py rings) and, in this arrangement, the polyfluoroaryl rings are not parallel but have an interplanar angle of 6.703 (3)°, as shown in Fig. 5. The *ortho*-Br atoms of both molecules are on the same side (as shown in the inset of Fig. 5), resulting in significant steric hindrance on one side. Consequently, the polyfluoroaryl rings are tilted at an angle of 6.703 (3)° to reduce the steric hindrance. The inter-centroid distance is 3.7969 (10) Å and the rings are offset by 1.7513 (15) Å, as was also observed for other similar compounds (Ojha *et al.*, 2018). On the other hand, in **1*p***, a π–π interaction was observed between two pyridine rings, and not between polyfluoroaryl rings.

The π–π interaction is further anchored by strong intermolecular hydrogen bonding between the *para*-F atom of **1*ox*** with a methylene H of the ligand backbone of **1*oy***, and *vice*

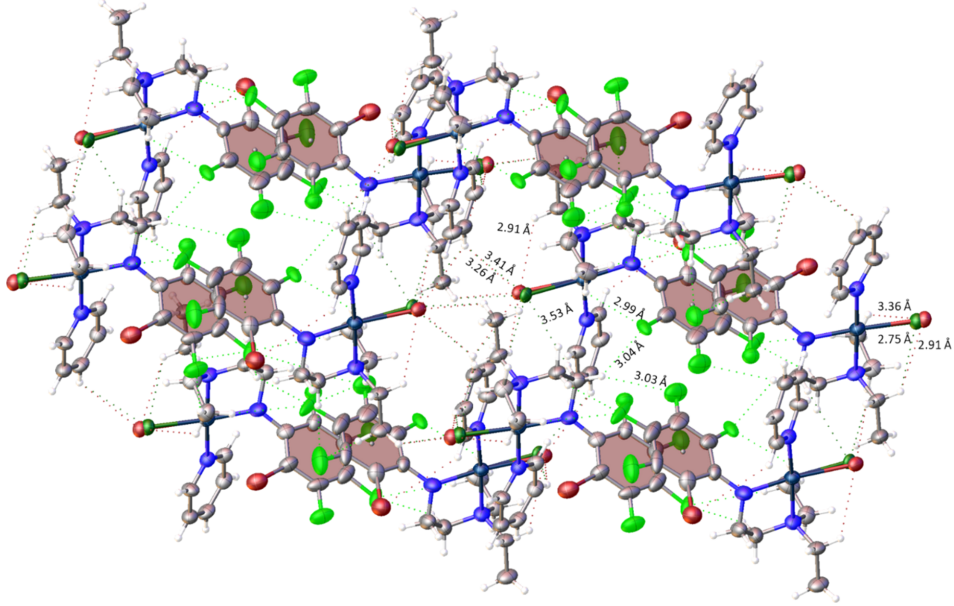

Figure 7
The crystal packing in **1*ox***/**1*oy***, showing $H\cdots Cl$ interactions for **1*ox*** and $C\cdots H$ interactions for **1*oy*** as intermolecular hydrogen bonding.

versa, as shown in Fig. 6, with H···F distances of 2.352 (7) and 2.424 (10) Å. Additionally, comparatively weak interactions, such as between the *para*-F atom of **1*ox*** with a methyl H atom of the NEt_2 group, with an H···F distance of 3.012 (8) Å, and a very weak interaction between the *ortho*-F atom of **1*ox*** and a methylene H atom of the ligand backbone of **1*oy***, with a H···F distance of 3.353 (11) Å, further stabilize the π–π interaction.

In the **1*ox*/1*oy*** isomers, one Et group makes an agostic interaction with Pt; the Pt···H(CH_3) distance is 2.8043 (11) Å and the bond angles are 118.8 (3)° for H—Pt—N(py), 103.8 (3)° for H—Pt—N(C_6F_5) and 65.3 (3)° for H—Pt—N($Et)_2$ in **1*ox***, and the Pt···H(CH_3) distance is 3.0032 (11) Å and the bond angles are 120.0 (3)° for H—Pt—N(py), 106.7 (3)° for H—Pt—N(C_6F_5) and 66.1 (3)° for H—Pt—N($Et)_2$ in **1*oy***. The *ortho*-F atom of **1*ox*** makes an intramolecular hydrogen-bonding contact with a methyl H atom of –N(Et_2), which exhibits an agostic interaction with Pt, with an H···F distance of 2.994 (7) Å (Fig. 7). These rotamers display the entire network of supramolecular interactions, as illustrated in Fig. 7. The *p*-H(py) atom of **1*ox*** is anchored by intermolecular hydrogen bonding with the Cl/Br atom of the two adjacent **1*ox*** molecules, with H···Br distances of 3.050 (16) and 3.26 (2) Å, and H···Cl distances of 3.15 (2) and 3.41 (3) Å (see Fig. 7). Similarly, the *m*-H(py) atom is involved in hydrogen bonding with the Cl/Br atom of another **1*ox*** molecule, with a H···Br distance of 2.78 (4) Å and a H···Cl distance of 2.578 (8) Å.

Intermolecular F···H hydrogen bonding of two adjacent **1*ox*** molecules, with an F···H distance of 2.915 (9) Å, was observed between the *m*-F atom of the polyfluoroaryl ring and a methyl H of the Et group (–NEt_2), the one not showing the agostic interactions with Pt (Fig. 7). These supramolecular interactions may facilitate the docking of the drug and reinforce the nucleobase–Pt interactions.

4. Conclusion

Further examination of the products of the reaction between [$PtCl_2${$H_2N(CH_2)_2NEt_2$}], Tl_2CO_3 and bromopentafluorobenzene in refluxing pyridine has revealed that, in addition to the major product, [Pt{(*p*-BrC_6F_4)$N(CH_2)_2NEt_2$}Cl(py)], *i.e.* **1*p***, a significant amount of the *ortho*-stereoisomer, [Pt{(*o*-BrC_6F_4)$N(CH_2)_2NEt_2$}Cl(py)], *i.e.* **1*o***, can also be isolated, taking advantage of the much higher solubility of **1*o***. The new regioisomer, which was characterized by synchrotron X-ray crystallography, crystallizes as a 1:1 mixture of two rotameric isomers, *i.e.* **1*ox*** and **1*oy***, according to whether the Br substituent and the Cl ligand are in an *anti* (in **1*ox***) or *syn* (in **1*oy***) disposition. The ^{1}H and ^{19}F NMR spectra in $(CD_3)_2CO$ are consistent with the structural assignment.

Acknowledgements

AMB gratefully acknowledges financial support from the Australian Research Council. RO thanks the Australian Government for the provision of an Australian Postgraduate Award. All the authors thank Dr Craig M. Forsyth for his help in the refinement of the crystal data. X-ray crystallography data collection in this research was undertaken on the MX1 beamline at the Australian Synchrotron, which is a part of ANSTO (Cowieson *et al.*, 2015). Open access publishing facilitated by Monash University, as part of the Wiley–Monash University agreement via the Council of Australian University Librarians.

Funding information

Funding for this research was provided by: Australian Research Council (grant No. DP120101470).

References

Ando, S. & Matsuura, T. (1995). *Magn. Reson. Chem.* **33**, 639–645.
Ault, J. L., Harries, H. J. & Burgess, J. (1977). *Inorg. Chim. Acta* **25**, 65–69.
Battle, A. R., Bond, A. M., Chow, A., Daniels, D. P., Deacon, G. B., Hambley, T. W., Junk, P. C., Mason, D. N. & Wang, J. (2010). *J. Fluor. Chem.* **131**, 1229–1236.
Bruce, M. I. (1968). *J. Chem. Soc. A* pp. 1459–1464.
Buxton, D. P., Deacon, G. B., Gatehouse, B. M., Grayson, I. L. & Black, D. S. C. (1988). *Aust. J. Chem.* **41**, 943–956.
Chambers, R. D. (2004). *Fluorine in Organic Chemistry*, pp. 122–136. Oxford: Blackwell Publishing Ltd.
Chambers, R. D., Musgrave, W. K. R., Waterhouse, J. S., Williams, D. L. H., Burdon, J., Hollyhead, W. B. & Tatlow, J. C. (1974). *J. Chem. Soc. Chem. Commun.* pp. 239–240.
Chambers, R. D., Waterhouse, J. S. & Williams, D. L. H. (1977). *J. Chem. Soc. Perkin Trans. 2*, pp. 585–588.
Cowieson, N. P., Aragao, D., Clift, M., Ericsson, D. J., Gee, C., Harrop, S. J., Mudie, N., Panjikar, S., Price, J. R., Riboldi-Tunnicliffe, A., Williamson, R. & Caradoc-Davies, T. (2015). *J. Synchrotron Rad.* **22**, 187–190.
Deacon, G. B., Gatehouse, B. M., Haubrich, S. T., Ireland, J. & Lawrenz, E. T. (1998). *Polyhedron* **17**, 791–802.
Deacon, G. B., Gatehouse, B. M. & Ireland, J. (1991). *Aust. J. Chem.* **44**, 1669–1681.
Dolomanov, O. V., Bourhis, L. J., Gildea, R. J., Howard, J. A. K. & Puschmann, H. (2009). *J. Appl. Cryst.* **42**, 339–341.
Kabsch, W. (1993). *J. Appl. Cryst.* **26**, 795–800.
McPhillips, T. M., McPhillips, S. E., Chiu, H.-J., Cohen, A. E., Deacon, A. M., Ellis, P. J., Garman, E., Gonzalez, A., Sauter, N. K., Phizackerley, R. P., Soltis, S. M. & Kuhn, P. (2002). *J. Synchrotron Rad.* **9**, 401–406.
Ojha, R., Boas, J. F., Deacon, G. B., Junk, P. C. & Bond, A. M. (2016). *J. Inorg. Biochem.* **162**, 194–200.
Ojha, R., Junk, P. C., Bond, A. M. & Deacon, G. B. (2023). *Molecules* **28**, 6402.
Ojha, R., Junk, P. C., Deacon, G. B. & Bond, A. M. (2018). *Supramol. Chem.* **30**, 418–424.
Ojha, R., Mason, D., Forsyth, C. M., Deacon, G. B., Junk, P. C. & Bond, A. M. (2021). *J. Inorg. Biochem.* **218**, 111360.
Ojha, R., Nafady, A., Shiddiky, M. J. A., Mason, D., Boas, J. F., Torriero, A. A. J., Bond, A. M., Deacon, G. B. & Junk, P. C. (2015). *ChemElectroChem* **2**, 1048–1061.
Sheldrick, G. M. (2015*a*). *Acta Cryst.* A**71**, 3–8.
Sheldrick, G. M. (2015*b*). *Acta Cryst.* C**71**, 3–8.
Talarico, T., Phillips, D. R., Deacon, G. B., Rainone, S. & Webster, L. K. (1999). *Invest. New Drugs* **17**, 1–15.

supporting information

Acta Cryst. (2025). C**81**, 513-518 [https://doi.org/10.1107/S2053229625006837]

Syn- and *anti*-rotamers of the *ortho*-stereoisomer [Pt{(*o*-BrC_6F_4)$N(CH_2)_2NEt_2$}Cl(py)]

Ruchika Ojha, Alan M. Bond, Peter C. Junk and Glen B. Deacon

Computing details

***trans*-[*N*-(2-Bromo-3,4,5,6-tetrafluorophenyl)-*N*′,*N*′-diethylethane-1,2-diaminato(1-)]chloridopyridineplatinum(II)**

Crystal data

$[PtBr_{0.1}(C_{12}H_{14}BrF_4N_2)(C_5H_5N)Cl_{0.9}]$
$[PtBr_{0.4}(C_{12}H_{14}BrF_4N_2)(C_5H_5N)Cl_{0.6}]$
M_r = 1321.39
Triclinic, $P\overline{1}$
a = 9.4810 (19) Å
b = 14.656 (3) Å
c = 15.094 (3) Å
α = 75.02 (3)°
β = 74.62 (3)°
γ = 86.28 (3)°
V = 1953.5 (8) Å^3
Z = 2
$F(000)$ = 1246
D_x = 2.246 Mg m^{-3}
Synchrotron radiation, λ = 0.7108 Å
Cell parameters from 8572 reflections
θ = 1.4–27.9°
μ = 9.79 mm^{-1}
T = 100 K
Prism, yellow
0.02 × 0.02 × 0.01 mm

Data collection

ADSC Quantum 210r diffractometer
Radiation source: Australian Synchrotron MX1
phi scans
24773 measured reflections
8572 independent reflections
6722 reflections with $I > 2\sigma(I)$
R_{int} = 0.055
θ_{max} = 27.9°, θ_{min} = 1.4°
h = −12→12
k = −19→19
l = −19→19
8572 standard reflections every 0 reflections
intensity decay: none

Refinement

Refinement on F^2
Least-squares matrix: full
$R[F^2 > 2\sigma(F^2)]$ = 0.063
$wR(F^2)$ = 0.174
S = 1.05
8572 reflections
506 parameters
38 restraints
Primary atom site location: dual
Hydrogen site location: inferred from neighbouring sites
H-atom parameters constrained
$w = 1/[\sigma^2(F_o^2) + (0.0879P)^2 + 22.6555P]$ where $P = (F_o^2 + 2F_c^2)/3$
$(\Delta/\sigma)_{max}$ = 0.001
$\Delta\rho_{max}$ = 2.78 e Å^{-3}
$\Delta\rho_{min}$ = −2.37 e Å^{-3}
Extinction correction: SHELXL2018 (Sheldrick, 2015*b*), $Fc^*=kFc[1+0.001xFc^2\lambda^3/\sin(2\theta)]^{-1/4}$
Extinction coefficient: 0.0085 (5)

Special details

Geometry. All e.s.d.'s (except the e.s.d. in the dihedral angle between two l.s. planes) are estimated using the full covariance matrix. The cell e.s.d.'s are taken into account individually in the estimation of e.s.d.'s in distances, angles and torsion angles; correlations between e.s.d.'s in cell parameters are only used when they are defined by crystal symmetry. An approximate (isotropic) treatment of cell e.s.d.'s is used for estimating e.s.d.'s involving l.s. planes.

Fractional atomic coordinates and isotropic or equivalent isotropic displacement parameters (Å²)

	x	*y*	*z*	U_{iso}*/U_{eq}	Occ. (<1)
Pt1	0.68588 (5)	0.26255 (3)	0.69629 (3)	0.03652 (16)	
Pt2	0.84692 (4)	0.40034 (3)	0.21031 (3)	0.03580 (16)	
Br1	0.29324 (18)	0.10436 (12)	0.96603 (11)	0.0617 (4)	
Br2	0.76261 (16)	0.27209 (12)	0.07351 (11)	0.0582 (4)	
Br1A	0.844 (2)	0.4020 (10)	0.5902 (13)	0.036 (2)	0.414 (11)
Br2A	1.011 (5)	0.549 (2)	0.112 (3)	0.0371 (12)	0.091 (10)
F1	0.1118 (10)	−0.0192 (6)	0.9139 (9)	0.083 (3)	
F2	0.1215 (11)	−0.0589 (5)	0.7548 (8)	0.085 (3)	
F3	0.3670 (13)	0.0166 (6)	0.5945 (8)	0.078 (3)	
F4	0.5838 (7)	0.1069 (5)	0.6057 (5)	0.0454 (17)	
F5	0.5008 (10)	0.1702 (7)	0.0865 (6)	0.065 (2)	
F6	0.2804 (7)	0.0882 (4)	0.2309 (6)	0.0478 (18)	
F7	0.2840 (9)	0.1086 (6)	0.4125 (6)	0.062 (2)	
F8	0.4821 (8)	0.2093 (5)	0.4402 (5)	0.0447 (16)	
N1	0.5650 (12)	0.1575 (8)	0.7918 (8)	0.048 (3)	
N2	0.8564 (11)	0.1972 (7)	0.7524 (7)	0.040 (2)	
N3	0.5077 (10)	0.3228 (7)	0.6537 (7)	0.036 (2)	
N4	0.7279 (12)	0.2856 (8)	0.2896 (8)	0.048 (3)	
N5	1.0108 (10)	0.3299 (7)	0.2689 (8)	0.041 (2)	
N6	0.6742 (10)	0.4682 (7)	0.1676 (7)	0.0348 (19)	
C1	0.3369 (12)	0.0695 (9)	0.8536 (10)	0.049 (3)	
C2	0.2294 (14)	0.0143 (8)	0.8452 (10)	0.058 (4)	
C3	0.2381 (17)	−0.0042 (10)	0.7587 (10)	0.072 (5)	
C4	0.3514 (14)	0.0330 (10)	0.6810 (12)	0.072 (5)	
C5	0.4619 (16)	0.0853 (9)	0.6918 (10)	0.052 (3)	
C6	0.4588 (12)	0.1060 (8)	0.7783 (8)	0.041 (3)	
C7	0.6381 (14)	0.1128 (10)	0.8651 (9)	0.048 (3)	
H7A	0.593910	0.050255	0.900527	0.057*	
H7B	0.629319	0.152434	0.910403	0.057*	
C8	0.7960 (14)	0.1022 (9)	0.8160 (10)	0.047 (3)	
H8A	0.804889	0.055707	0.777419	0.056*	
H8B	0.852798	0.078673	0.863654	0.056*	
C9	0.8925 (15)	0.2589 (10)	0.8095 (10)	0.047 (3)	
H9A	0.801059	0.270905	0.854930	0.056*	
H9B	0.928483	0.320540	0.765718	0.056*	
C10	1.0060 (16)	0.2195 (10)	0.8650 (11)	0.054 (3)	
H10A	1.095621	0.203945	0.821542	0.082*	
H10B	0.967023	0.162426	0.914066	0.082*	
H10C	1.028032	0.266938	0.894813	0.082*	

C11	0.9930 (14)	0.1841 (10)	0.6768 (10)	0.048 (3)
H11A	1.037998	0.246810	0.643044	0.058*
H11B	1.064064	0.145908	0.708542	0.058*
C12	0.9669 (17)	0.1370 (11)	0.6047 (10)	0.056 (3)
H12A	1.057406	0.138283	0.554506	0.084*
H12B	0.889970	0.170742	0.576982	0.084*
H12C	0.936461	0.071332	0.635813	0.084*
C13	0.3853 (12)	0.3349 (8)	0.7196 (8)	0.037 (2)
H13	0.383238	0.312461	0.784832	0.044*
C14	0.2652 (13)	0.3781 (9)	0.6955 (9)	0.043 (3)
H14	0.180904	0.386731	0.743289	0.051*
C15	0.2668 (14)	0.4097 (9)	0.5995 (9)	0.045 (3)
H15	0.183628	0.439585	0.580795	0.054*
C16	0.3898 (13)	0.3966 (10)	0.5339 (10)	0.046 (3)
H16	0.393144	0.417337	0.468304	0.055*
C17	0.5108 (13)	0.3533 (9)	0.5618 (8)	0.039 (2)
H17	0.596855	0.345227	0.515042	0.047*
C18	0.5011 (11)	0.1986 (8)	0.3484 (9)	0.041 (3)
C19	0.3930 (14)	0.1453 (10)	0.3386 (9)	0.052 (3)
C20	0.3927 (14)	0.1386 (9)	0.2490 (9)	0.056 (4)
C21	0.5055 (12)	0.1814 (9)	0.1724 (9)	0.049 (3)
C22	0.6140 (14)	0.2328 (10)	0.1837 (9)	0.048 (3)
C23	0.6197 (12)	0.2407 (9)	0.2731 (7)	0.040 (3)
C24	0.7917 (13)	0.2382 (9)	0.3686 (9)	0.042 (3)
H24A	0.750692	0.173742	0.398470	0.050*
H24B	0.771736	0.274514	0.417514	0.050*
C25	0.9527 (13)	0.2342 (9)	0.3248 (9)	0.044 (3)
H25A	1.004040	0.209574	0.375300	0.053*
H25B	0.971497	0.190623	0.282661	0.053*
C26	1.0383 (14)	0.3876 (9)	0.3331 (9)	0.044 (3)
H26A	0.944977	0.392396	0.380404	0.053*
H26B	1.066652	0.452355	0.294031	0.053*
C27	1.1553 (16)	0.3502 (11)	0.3865 (11)	0.056 (4)
H27A	1.251437	0.354006	0.340966	0.084*
H27B	1.133435	0.284230	0.421567	0.084*
H27C	1.155826	0.388277	0.431002	0.084*
C28	1.1543 (13)	0.3234 (10)	0.1954 (10)	0.044 (3)
H28A	1.222347	0.281796	0.227181	0.053*
H28B	1.199440	0.386960	0.168609	0.053*
C29	1.1344 (14)	0.2848 (10)	0.1138 (10)	0.050 (3)
H29A	1.093553	0.334224	0.070248	0.075*
H29B	1.067544	0.230496	0.139831	0.075*
H29C	1.229399	0.264957	0.079482	0.075*
C30	0.5450 (12)	0.4683 (9)	0.2321 (8)	0.039 (2)
H30	0.536734	0.433241	0.295741	0.047*
C31	0.4239 (13)	0.5171 (8)	0.2102 (9)	0.041 (3)
H31	0.334751	0.515894	0.257648	0.050*
C32	0.4356 (13)	0.5677 (9)	0.1176 (10)	0.045 (3)

H32	0.354726	0.602666	0.100600	0.055*	
C33	0.5671 (13)	0.5669 (9)	0.0493 (9)	0.043 (3)	
H33	0.575966	0.599672	−0.015072	0.051*	
C34	0.6869 (14)	0.5168 (9)	0.0768 (9)	0.044 (3)	
H34	0.777604	0.517330	0.030862	0.053*	
Cl1	0.837 (3)	0.3837 (16)	0.586 (2)	0.030 (3)	0.586 (11)
Cl2	0.9986 (9)	0.5287 (5)	0.1236 (6)	0.0371 (12)	0.909 (10)

Atomic displacement parameters (Å²)

	U^{11}	U^{22}	U^{33}	U^{12}	U^{13}	U^{23}
Pt1	0.0295 (2)	0.0424 (3)	0.0387 (3)	0.00454 (19)	−0.01210 (17)	−0.00950 (18)
Pt2	0.0266 (2)	0.0453 (3)	0.0386 (3)	0.00293 (19)	−0.01070 (16)	−0.01434 (19)
Br1	0.0605 (9)	0.0669 (9)	0.0567 (8)	−0.0041 (7)	−0.0199 (7)	−0.0080 (7)
Br2	0.0504 (8)	0.0756 (10)	0.0541 (8)	0.0061 (7)	−0.0173 (6)	−0.0233 (7)
Br1A	0.041 (3)	0.030 (6)	0.044 (2)	0.006 (4)	−0.0188 (18)	−0.014 (3)
Br2A	0.031 (2)	0.037 (3)	0.042 (3)	−0.002 (2)	−0.0059 (18)	−0.010 (3)
F1	0.050 (5)	0.052 (5)	0.127 (9)	−0.010 (4)	−0.006 (5)	0.000 (5)
F3	0.115 (9)	0.053 (5)	0.092 (7)	0.015 (5)	−0.056 (7)	−0.036 (5)
F5	0.072 (6)	0.079 (6)	0.068 (6)	0.017 (5)	−0.039 (5)	−0.041 (5)
F6	0.029 (3)	0.026 (3)	0.093 (6)	−0.001 (3)	−0.026 (3)	−0.013 (3)
F7	0.052 (5)	0.056 (5)	0.070 (6)	−0.007 (4)	−0.017 (4)	0.000 (4)
F8	0.051 (4)	0.044 (4)	0.043 (4)	0.003 (3)	−0.017 (3)	−0.014 (3)
N1	0.040 (6)	0.057 (6)	0.046 (6)	0.002 (5)	−0.019 (5)	−0.003 (5)
N2	0.035 (5)	0.038 (5)	0.049 (6)	0.009 (4)	−0.018 (4)	−0.009 (4)
N3	0.029 (5)	0.035 (5)	0.046 (5)	0.008 (4)	−0.013 (4)	−0.013 (4)
N4	0.038 (6)	0.060 (7)	0.049 (6)	−0.001 (5)	−0.022 (5)	−0.008 (5)
N5	0.026 (5)	0.048 (6)	0.055 (6)	0.014 (4)	−0.021 (4)	−0.018 (5)
N6	0.025 (4)	0.039 (5)	0.042 (5)	0.005 (4)	−0.007 (4)	−0.015 (4)
C1	0.038 (7)	0.040 (6)	0.065 (9)	0.010 (6)	−0.004 (6)	−0.019 (6)
C2	0.032 (7)	0.026 (6)	0.109 (13)	0.000 (5)	−0.019 (7)	−0.002 (7)
C3	0.068 (11)	0.040 (7)	0.128 (17)	0.004 (8)	−0.057 (11)	−0.024 (9)
C4	0.065 (11)	0.054 (9)	0.116 (15)	0.020 (8)	−0.063 (11)	−0.018 (10)
C5	0.058 (9)	0.042 (7)	0.066 (9)	0.010 (6)	−0.035 (7)	−0.015 (6)
C6	0.034 (6)	0.033 (5)	0.056 (7)	−0.002 (5)	−0.017 (5)	−0.004 (5)
C7	0.037 (6)	0.060 (8)	0.043 (7)	−0.007 (6)	−0.013 (5)	−0.004 (6)
C8	0.044 (7)	0.043 (6)	0.051 (7)	−0.006 (6)	−0.018 (6)	0.001 (5)
C9	0.044 (7)	0.052 (7)	0.050 (7)	0.005 (6)	−0.028 (6)	−0.008 (6)
C10	0.050 (8)	0.055 (8)	0.071 (9)	0.017 (7)	−0.037 (7)	−0.020 (7)
C11	0.037 (7)	0.045 (7)	0.064 (8)	0.011 (6)	−0.015 (6)	−0.016 (6)
C12	0.054 (8)	0.057 (8)	0.054 (8)	0.030 (7)	−0.015 (6)	−0.016 (6)
C13	0.029 (5)	0.040 (6)	0.042 (6)	0.006 (5)	−0.010 (4)	−0.012 (5)
C14	0.026 (5)	0.058 (7)	0.051 (7)	0.007 (5)	−0.014 (5)	−0.024 (6)
C15	0.042 (7)	0.046 (7)	0.054 (7)	0.003 (6)	−0.023 (6)	−0.013 (6)
C16	0.030 (6)	0.064 (8)	0.052 (7)	0.012 (6)	−0.019 (5)	−0.023 (6)
C17	0.032 (6)	0.054 (7)	0.033 (6)	0.011 (5)	−0.011 (4)	−0.014 (5)
C18	0.029 (6)	0.038 (6)	0.058 (7)	0.003 (5)	−0.011 (5)	−0.015 (5)
C19	0.037 (7)	0.053 (8)	0.066 (9)	−0.004 (6)	−0.018 (6)	−0.008 (6)

C20	0.050 (8)	0.040 (7)	0.097 (12)	0.011 (6)	−0.042 (8)	−0.031 (7)
C21	0.057 (8)	0.054 (7)	0.057 (8)	0.026 (7)	−0.036 (7)	−0.033 (7)
C22	0.042 (7)	0.058 (8)	0.055 (8)	0.007 (6)	−0.020 (6)	−0.027 (6)
C23	0.025 (5)	0.047 (6)	0.051 (7)	0.012 (5)	−0.012 (5)	−0.016 (5)
C24	0.030 (6)	0.052 (7)	0.042 (6)	0.006 (5)	−0.008 (5)	−0.015 (5)
C25	0.039 (6)	0.050 (7)	0.049 (7)	0.002 (6)	−0.022 (5)	−0.011 (6)
C26	0.041 (7)	0.053 (7)	0.049 (7)	0.003 (6)	−0.022 (5)	−0.021 (6)
C27	0.057 (8)	0.058 (8)	0.058 (8)	−0.010 (7)	−0.032 (7)	−0.004 (7)
C28	0.026 (5)	0.050 (7)	0.060 (8)	0.018 (5)	−0.010 (5)	−0.023 (6)
C29	0.036 (6)	0.058 (8)	0.055 (8)	−0.003 (6)	−0.007 (5)	−0.018 (6)
C30	0.026 (5)	0.053 (7)	0.039 (6)	0.005 (5)	−0.005 (4)	−0.018 (5)
C31	0.028 (6)	0.041 (6)	0.058 (7)	0.009 (5)	−0.012 (5)	−0.018 (5)
C32	0.031 (6)	0.050 (7)	0.065 (8)	0.009 (6)	−0.024 (5)	−0.020 (6)
C33	0.039 (6)	0.043 (6)	0.049 (7)	0.003 (5)	−0.021 (5)	−0.007 (5)
C34	0.033 (6)	0.054 (7)	0.043 (6)	0.005 (6)	−0.017 (5)	−0.002 (5)
Cl1	0.034 (4)	0.020 (6)	0.042 (4)	0.001 (4)	−0.012 (3)	−0.014 (4)
F4	0.028 (3)	0.043 (4)	0.052 (4)	−0.001 (3)	−0.015 (3)	0.017 (3)
F2	0.092 (7)	0.032 (4)	0.177 (10)	0.015 (4)	−0.103 (7)	−0.042 (5)
Cl2	0.031 (2)	0.037 (3)	0.042 (3)	−0.002 (2)	−0.0059 (18)	−0.010 (3)

Geometric parameters (Å, º)

Pt1—N1	1.993 (11)	C10—H10B	0.9800
Pt1—N3	2.034 (9)	C10—H10C	0.9800
Pt1—N2	2.087 (10)	C11—C12	1.508 (19)
Pt1—Cl1	2.35 (3)	C11—H11A	0.9900
Pt1—Br1A	2.534 (16)	C11—H11B	0.9900
Pt2—N4	2.006 (11)	C12—H12A	0.9800
Pt2—N6	2.026 (9)	C12—H12B	0.9800
Pt2—N5	2.076 (9)	C12—H12C	0.9800
Pt2—Cl2	2.323 (7)	C13—C14	1.355 (16)
Pt2—Br2A	2.62 (3)	C13—H13	0.9500
Br1—C1	1.833 (13)	C14—C15	1.399 (18)
Br2—C22	1.858 (14)	C14—H14	0.9500
F1—C2	1.324 (16)	C15—C16	1.354 (18)
F3—C4	1.36 (2)	C15—H15	0.9500
F5—C21	1.360 (13)	C16—C17	1.386 (16)
F6—C20	1.454 (13)	C16—H16	0.9500
F7—C19	1.324 (15)	C17—H17	0.9500
F8—C18	1.396 (14)	C18—C19	1.388 (11)
N1—C6	1.382 (15)	C18—C23	1.409 (11)
N1—C7	1.452 (15)	C19—C20	1.381 (12)
N2—C9	1.510 (16)	C20—C21	1.390 (12)
N2—C8	1.519 (15)	C21—C22	1.383 (11)
N2—C11	1.521 (17)	C22—C23	1.400 (12)
N3—C17	1.336 (14)	C24—C25	1.498 (17)
N3—C13	1.349 (14)	C24—H24A	0.9900
N4—C23	1.361 (15)	C24—H24B	0.9900

N4—C24	1.474 (15)	C25—H25A	0.9900
N5—C25	1.491 (16)	C25—H25B	0.9900
N5—C26	1.518 (14)	C26—C27	1.532 (17)
N5—C28	1.526 (15)	C26—H26A	0.9900
N6—C34	1.348 (15)	C26—H26B	0.9900
N6—C30	1.349 (14)	C27—H27A	0.9800
C1—C2	1.392 (12)	C27—H27B	0.9800
C1—C6	1.408 (12)	C27—H27C	0.9800
C2—C3	1.381 (13)	C28—C29	1.539 (18)
C3—C4	1.380 (14)	C28—H28A	0.9900
C3—F2	1.430 (15)	C28—H28B	0.9900
C4—C5	1.403 (12)	C29—H29A	0.9800
C5—C6	1.408 (12)	C29—H29B	0.9800
C5—F4	1.471 (16)	C29—H29C	0.9800
C7—C8	1.502 (18)	C30—C31	1.382 (16)
C7—H7A	0.9900	C30—H30	0.9500
C7—H7B	0.9900	C31—C32	1.381 (19)
C8—H8A	0.9900	C31—H31	0.9500
C8—H8B	0.9900	C32—C33	1.393 (18)
C9—C10	1.530 (16)	C32—H32	0.9500
C9—H9A	0.9900	C33—C34	1.408 (16)
C9—H9B	0.9900	C33—H33	0.9500
C10—H10A	0.9800	C34—H34	0.9500

N1—Pt1—N3	91.6 (4)	H11A—C11—H11B	107.6
N1—Pt1—N2	84.2 (4)	C11—C12—H12A	109.5
N3—Pt1—N2	174.8 (4)	C11—C12—H12B	109.5
N1—Pt1—Cl1	177.5 (9)	H12A—C12—H12B	109.5
N3—Pt1—Cl1	90.9 (8)	C11—C12—H12C	109.5
N2—Pt1—Cl1	93.3 (8)	H12A—C12—H12C	109.5
N1—Pt1—Br1A	173.7 (5)	H12B—C12—H12C	109.5
N3—Pt1—Br1A	90.8 (5)	N3—C13—C14	122.0 (11)
N2—Pt1—Br1A	93.0 (5)	N3—C13—H13	119.0
Cl1—Pt1—Br1A	5.7 (9)	C14—C13—H13	119.0
N4—Pt2—N6	93.2 (4)	C13—C14—C15	119.2 (12)
N4—Pt2—N5	83.5 (4)	C13—C14—H14	120.4
N6—Pt2—N5	173.9 (4)	C15—C14—H14	120.4
N4—Pt2—Cl2	175.8 (4)	C16—C15—C14	118.4 (12)
N6—Pt2—Cl2	90.9 (4)	C16—C15—H15	120.8
N5—Pt2—Cl2	92.3 (4)	C14—C15—H15	120.8
N4—Pt2—Br2A	177.2 (11)	C15—C16—C17	120.5 (12)
N6—Pt2—Br2A	89.3 (10)	C15—C16—H16	119.8
N5—Pt2—Br2A	93.9 (10)	C17—C16—H16	119.8
Cl2—Pt2—Br2A	1.8 (12)	N3—C17—C16	120.7 (11)
C6—N1—C7	117.8 (11)	N3—C17—H17	119.7
C6—N1—Pt1	126.9 (8)	C16—C17—H17	119.7
C7—N1—Pt1	110.9 (8)	C19—C18—F8	114.3 (9)
C9—N2—C8	111.0 (10)	C19—C18—C23	124.0 (11)

C9—N2—C11	109.3 (10)	F8—C18—C23	121.7 (9)
C8—N2—C11	110.6 (10)	F7—C19—C20	120.1 (9)
C9—N2—Pt1	107.0 (7)	F7—C19—C18	120.6 (10)
C8—N2—Pt1	105.6 (7)	C20—C19—C18	119.0 (12)
C11—N2—Pt1	113.3 (8)	C19—C20—C21	118.6 (11)
C17—N3—C13	119.3 (10)	C19—C20—F6	123.1 (10)
C17—N3—Pt1	121.4 (8)	C21—C20—F6	118.2 (9)
C13—N3—Pt1	119.3 (8)	F5—C21—C22	122.8 (11)
C23—N4—C24	118.6 (11)	F5—C21—C20	115.7 (9)
C23—N4—Pt2	130.7 (8)	C22—C21—C20	121.5 (11)
C24—N4—Pt2	109.7 (7)	C21—C22—C23	121.8 (12)
C25—N5—C26	111.1 (10)	C21—C22—Br2	113.4 (8)
C25—N5—C28	111.2 (10)	C23—C22—Br2	124.1 (8)
C26—N5—C28	108.2 (9)	N4—C23—C22	124.7 (10)
C25—N5—Pt2	107.0 (7)	N4—C23—C18	120.6 (10)
C26—N5—Pt2	105.7 (7)	C22—C23—C18	114.7 (10)
C28—N5—Pt2	113.5 (8)	N4—C24—C25	105.2 (10)
C34—N6—C30	119.0 (10)	N4—C24—H24A	110.7
C34—N6—Pt2	121.6 (8)	C25—C24—H24A	110.7
C30—N6—Pt2	119.3 (8)	N4—C24—H24B	110.7
C2—C1—C6	123.3 (12)	C25—C24—H24B	110.7
C2—C1—Br1	113.9 (9)	H24A—C24—H24B	108.8
C6—C1—Br1	122.3 (8)	N5—C25—C24	110.7 (10)
F1—C2—C3	115.7 (11)	N5—C25—H25A	109.5
F1—C2—C1	124.7 (12)	C24—C25—H25A	109.5
C3—C2—C1	119.4 (13)	N5—C25—H25B	109.5
C4—C3—C2	120.2 (13)	C24—C25—H25B	109.5
C4—C3—F2	123.5 (11)	H25A—C25—H25B	108.1
C2—C3—F2	116.3 (11)	N5—C26—C27	116.4 (11)
F3—C4—C3	123.0 (11)	N5—C26—H26A	108.2
F3—C4—C5	117.4 (13)	C27—C26—H26A	108.2
C3—C4—C5	119.5 (15)	N5—C26—H26B	108.2
C4—C5—C6	122.7 (13)	C27—C26—H26B	108.2
C4—C5—F4	111.8 (11)	H26A—C26—H26B	107.3
C6—C5—F4	125.3 (10)	C26—C27—H27A	109.5
N1—C6—C5	124.5 (10)	C26—C27—H27B	109.5
N1—C6—C1	120.6 (10)	H27A—C27—H27B	109.5
C5—C6—C1	114.8 (11)	C26—C27—H27C	109.5
N1—C7—C8	106.9 (11)	H27A—C27—H27C	109.5
N1—C7—H7A	110.3	H27B—C27—H27C	109.5
C8—C7—H7A	110.3	N5—C28—C29	113.1 (10)
N1—C7—H7B	110.3	N5—C28—H28A	109.0
C8—C7—H7B	110.3	C29—C28—H28A	109.0
H7A—C7—H7B	108.6	N5—C28—H28B	109.0
C7—C8—N2	109.4 (11)	C29—C28—H28B	109.0
C7—C8—H8A	109.8	H28A—C28—H28B	107.8
N2—C8—H8A	109.8	C28—C29—H29A	109.5
C7—C8—H8B	109.8	C28—C29—H29B	109.5

N2—C8—H8B	109.8	H29A—C29—H29B	109.5
H8A—C8—H8B	108.2	C28—C29—H29C	109.5
N2—C9—C10	115.8 (11)	H29A—C29—H29C	109.5
N2—C9—H9A	108.3	H29B—C29—H29C	109.5
C10—C9—H9A	108.3	N6—C30—C31	123.1 (11)
N2—C9—H9B	108.3	N6—C30—H30	118.4
C10—C9—H9B	108.3	C31—C30—H30	118.4
H9A—C9—H9B	107.4	C32—C31—C30	118.4 (12)
C9—C10—H10A	109.5	C32—C31—H31	120.8
C9—C10—H10B	109.5	C30—C31—H31	120.8
H10A—C10—H10B	109.5	C31—C32—C33	119.4 (11)
C9—C10—H10C	109.5	C31—C32—H32	120.3
H10A—C10—H10C	109.5	C33—C32—H32	120.3
H10B—C10—H10C	109.5	C32—C33—C34	119.2 (12)
C12—C11—N2	114.6 (11)	C32—C33—H33	120.4
C12—C11—H11A	108.6	C34—C33—H33	120.4
N2—C11—H11A	108.6	N6—C34—C33	120.8 (12)
C12—C11—H11B	108.6	N6—C34—H34	119.6
N2—C11—H11B	108.6	C33—C34—H34	119.6

C6—C1—C2—F1	−178.4 (13)	F8—C18—C19—F7	−0.5 (19)
Br1—C1—C2—F1	−6.4 (18)	C23—C18—C19—F7	−179.5 (12)
C6—C1—C2—C3	−2 (2)	F8—C18—C19—C20	173.3 (11)
Br1—C1—C2—C3	169.9 (11)	C23—C18—C19—C20	−6 (2)
F1—C2—C3—C4	175.8 (14)	F7—C19—C20—C21	177.3 (13)
C1—C2—C3—C4	−1 (2)	C18—C19—C20—C21	3 (2)
F1—C2—C3—F2	−1.5 (19)	F7—C19—C20—F6	−3 (2)
C1—C2—C3—F2	−178.1 (12)	C18—C19—C20—F6	−177.0 (12)
C2—C3—C4—F3	179.2 (13)	C19—C20—C21—F5	178.4 (11)
F2—C3—C4—F3	−4 (2)	F6—C20—C21—F5	−1.1 (17)
C2—C3—C4—C5	3 (2)	C19—C20—C21—C22	−2 (2)
F2—C3—C4—C5	−179.5 (13)	F6—C20—C21—C22	178.2 (11)
F3—C4—C5—C6	−179.3 (12)	F5—C21—C22—C23	−177.7 (12)
C3—C4—C5—C6	−3 (2)	C20—C21—C22—C23	3 (2)
F3—C4—C5—F4	−4.5 (18)	F5—C21—C22—Br2	−6.9 (17)
C3—C4—C5—F4	171.5 (13)	C20—C21—C22—Br2	173.8 (11)
C7—N1—C6—C5	−122.4 (14)	C24—N4—C23—C22	−133.8 (13)
Pt1—N1—C6—C5	31.8 (18)	Pt2—N4—C23—C22	34.1 (19)
C7—N1—C6—C1	57.3 (17)	C24—N4—C23—C18	47.0 (17)
Pt1—N1—C6—C1	−148.4 (11)	Pt2—N4—C23—C18	−145.1 (11)
C4—C5—C6—N1	−179.7 (13)	C21—C22—C23—N4	176.1 (13)
F4—C5—C6—N1	6 (2)	Br2—C22—C23—N4	6.3 (19)
C4—C5—C6—C1	0.5 (19)	C21—C22—C23—C18	−4.7 (19)
F4—C5—C6—C1	−173.6 (12)	Br2—C22—C23—C18	−174.4 (10)
C2—C1—C6—N1	−177.5 (12)	C19—C18—C23—N4	−174.7 (13)
Br1—C1—C6—N1	11.1 (18)	F8—C18—C23—N4	6.4 (19)
C2—C1—C6—C5	2.2 (19)	C19—C18—C23—C22	6.1 (19)
Br1—C1—C6—C5	−169.2 (10)	F8—C18—C23—C22	−172.8 (11)

C6—N1—C7—C8	115.2 (12)	C23—N4—C24—C25	124.3 (12)
Pt1—N1—C7—C8	−43.0 (13)	Pt2—N4—C24—C25	−46.0 (11)
N1—C7—C8—N2	53.0 (14)	C26—N5—C25—C24	81.0 (11)
C9—N2—C8—C7	78.8 (12)	C28—N5—C25—C24	−158.4 (9)
C11—N2—C8—C7	−159.7 (10)	Pt2—N5—C25—C24	−33.9 (11)
Pt1—N2—C8—C7	−36.8 (11)	N4—C24—C25—N5	52.8 (13)
C8—N2—C9—C10	59.8 (15)	C25—N5—C26—C27	63.8 (14)
C11—N2—C9—C10	−62.5 (14)	C28—N5—C26—C27	−58.5 (14)
Pt1—N2—C9—C10	174.5 (10)	Pt2—N5—C26—C27	179.5 (10)
C9—N2—C11—C12	−170.6 (11)	C25—N5—C28—C29	69.7 (13)
C8—N2—C11—C12	66.9 (13)	C26—N5—C28—C29	−168.0 (11)
Pt1—N2—C11—C12	−51.4 (13)	Pt2—N5—C28—C29	−51.0 (13)
C17—N3—C13—C14	−0.7 (17)	C34—N6—C30—C31	−0.8 (17)
Pt1—N3—C13—C14	177.2 (9)	Pt2—N6—C30—C31	176.3 (9)
N3—C13—C14—C15	1.1 (18)	N6—C30—C31—C32	0.4 (18)
C13—C14—C15—C16	−0.6 (19)	C30—C31—C32—C33	1.0 (18)
C14—C15—C16—C17	−0.3 (19)	C31—C32—C33—C34	−2.0 (18)
C13—N3—C17—C16	−0.3 (17)	C30—N6—C34—C33	−0.2 (18)
Pt1—N3—C17—C16	−178.1 (9)	Pt2—N6—C34—C33	−177.3 (9)
C15—C16—C17—N3	1 (2)	C32—C33—C34—N6	1.6 (19)